Bulk electronic state of superconducting topological insulator

Tatsuki Hashimoto, Keiji Yada, Ai Yamakage, Masatoshi Sato, and Yukio Tanaka
Department of Applied Physics, Nagoya University, Nagoya 464-8603, Japan

We study electronic properties of a superconducting topological insulator whose parent material is a topological insulator. We calculate the temperature dependence of the specific heat and spin susceptibility for four promising superconducting pairings proposed by L. Fu and E. Berg (Phys. Rev. Lett. **105**, 097001). Since the line shapes of temperature dependence of specific heat are almost identical among three of the four pairings, it is difficult to identify them simply from the specific heat. On the other hand, we obtain wide varieties of the temperature dependence of spin susceptibility for each pairing reflecting the spin structure of Cooper pair. We propose that the pairing symmetry of superconducting topological insulator can be determined from measurement of Knight shift by changing the direction of applied magnetic field.

I. INTRODUCTION

Topological insulators (TIs) are new state of matter supporting massless Dirac fermions on the surface, which are characterized by non-zero topological numbers defined in the bulk.[1,2] Due to the surface Dirac fermions, TIs have potential to exhibit rich transport and electromagnetic response properties, which can be applicable for future devices. The superconducting analog of TI are topological superconductors,[2–6] which have Majorana fermions[7] on the surface as Andreev bound states (ABSs). In these materials, topological invariants can be defined in the bulk Hamiltonian. There are several types of topological superconductors, e.g., chiral p-wave superconducting state in Sr_2RuO_4,[8–11] helical superconducting state realized in non-centrosymmetric superconductors.[12,13] The realization of a topological superconductor is of particular interest in the viewpoint of quantum devices and quantum computations.[12–31]

Recently, carrier-doped TI $Cu_xBi_2Se_3$ is revealed to be a superconductor.[32] Hereafter, we refer to a superconductor based on TI as a superconducting topological insulator (STI). In the tunneling spectroscopy,[33] $Cu_xBi_2Se_3$ shows a zero-bias conductance peak (ZBCP). This means that $Cu_xBi_2Se_3$ can be regarded as a topological superconductor since the ZBCP signifies the existence of gapless ABSs[34–36] on the surface, which is a direct consequence of topological superconductivity. Interestingly, it has been clarified that the STI supports anomalous ABSs different from those of other topological superconductors,[29,37,38] and the resulting transport property also becomes anomalous.[29,38] In this sense, STIs are new type of topological superconductor, and has attracted much interest. Moreover, there are several experimental results supporting a generation of STI by the proximity effect.[39,40]

Nowadays, there are a lot of relevant studies about $Cu_xBi_2Se_3$.[32,33,41–47] However, up to now, the symmetry of superconductivity of $Cu_xBi_2Se_3$ still remains unknown. Although the specific heat has been measured, it is difficult to establish the superconducting symmetry only from the data of specific heat. More careful analysis with the help of the microscopic calculations is needed. In order to clarify the superconducting symmetry, it is useful to analyze spin susceptibility besides specific heat since the spin susceptibility is directly related to spin structure of superconducting pairing.

In this paper, we clarify the temperature dependences of specific heat and spin susceptibility for the possible superconducting pairings. Based on these quantities, it is possible to determine the pairing symmetry in a STI.

The paper is organized as follows. In Sec. II, we show the model Hamiltonian of STI, and give the energy spectra for the possible superconducting parings. The numerical results and discussion on the temperature dependences of the specific heat and spin susceptibility are shown in Sec. III, and Sec. IV, respectively. We compare our results of specific heat with the experimental data.[43] In Sec. V, we summarize our results and propose how to experimentally determine the superconducting symmetry of STI.

II. MODEL

For a model of STI, we start with the BdG Hamiltonian proposed in Ref.48,

$$H(\boldsymbol{k}) = H_0(\boldsymbol{k})\tau_z + \Delta_\ell \tau_x, \tag{1}$$

where $\ell = 1, 2, 3, 4$ represent the type of the pair potential. The normal part of the Hamiltonian $H_0(\boldsymbol{k})$ is low-energy effective model of a topologocal insulator,based on the $\boldsymbol{k}\cdot\boldsymbol{p}$ theory given by

$$\begin{aligned} H_0(\boldsymbol{k}) &= c(\boldsymbol{k}) + m(\boldsymbol{k})\sigma_x \\ &\quad + v_z k_z \sigma_y + v(k_x s_y - k_y s_x)\sigma_z, \quad (2)\\ m(\boldsymbol{k}) &= m_0 + m_1 k_z^2 + m_2(k_x^2 + k_y^2), \quad (3)\\ c(\boldsymbol{k}) &= -\mu + c_1 k_z^2 + c_2(k_x^2 + k_y^2). \quad (4) \end{aligned}$$

s_i, σ_i and τ_i $(i = x, y, z)$ are the Pauli matrices in spin, orbital and Nambu spaces, respectively. The basis of the orbitals are effective p_z orbitals constituted from p_z orbitals of Se and Bi p_z orbitals on the upper and lower side of the quintuple layer, as shown in Fig. 1. Hereafter, we call this basis "orbital basis". On the other hand, we refer

to the basis diagonalizing $H_0(\boldsymbol{k})$ as "band basis", which is introduced in Sec. IV B. In this model, the normal part $H_0(\boldsymbol{k})$ is equivalent to the model proposed in Ref.49 and Ref.50 under the unitary transformation. In the following, we use the tight-binding model which is equivalent to the above model at low energy. We consider the hexagonal lattice where two-dimensional triangular lattices stack along the c-axis.[33,37] Then, the tight-binding Hamiltonian is obtained by the following substitution in the $\boldsymbol{k}\cdot\boldsymbol{p}$ Hamiltonian Eqs. (2)-(4).

$$k_x \to \frac{2}{\sqrt{3}a}\sin\frac{\sqrt{3}k_x a}{2}\cos\frac{k_y a}{2} \equiv f_x(\boldsymbol{k}), \tag{5}$$

$$k_y \to \frac{2}{3a}(\cos\frac{\sqrt{3}k_x a}{2}\sin\frac{k_y a}{2} + \sin k_y a) \equiv f_y(\boldsymbol{k}), \tag{6}$$

$$k_z \to \frac{1}{c}\sin k_z c \equiv f_z(\boldsymbol{k}), \tag{7}$$

$$k_z^2 \to \frac{2}{c^2}(1-\cos k_z c) \equiv f_\perp(\boldsymbol{k}), \tag{8}$$

$$k_x^2+k_y^2 \to \frac{4}{3a^2}(3-2\cos\frac{\sqrt{3}k_x a}{2}\cos\frac{k_y a}{2}-\cos k_y a) \equiv f_\parallel(\boldsymbol{k}), \tag{9}$$

where a and c are the lattice constants. In this hexagonal lattice, the primitive lattice vectors are $(\sqrt{3}a/2, a/2, 0)$, $(0, a, 0)$, $(0, 0, c)$, though the actual crystal structure is not hexagonal but rhombohedral one.[49,50] This simplification does not affect the low energy excitations. Then, the normal part of the Hamiltonian is summarized as follows.

$$\begin{aligned} H_0(\boldsymbol{k}) &= c(\boldsymbol{k}) + m(\boldsymbol{k})\sigma_x \\ &\quad +(a_x(\boldsymbol{k})s_y - a_y(\boldsymbol{k})s_s)\sigma_z + b(\boldsymbol{k})\sigma_y, \quad (10)\\ c(\boldsymbol{k}) &= -\mu + c_1 f_\perp(\boldsymbol{k}) + c_2 f_\parallel(\boldsymbol{k}), \quad (11)\\ m(\boldsymbol{k}) &= m_0 + m_1 f_\perp(\boldsymbol{k}) + m_2 f_\parallel(\boldsymbol{k}), \quad (12)\\ a_{x,y}(\boldsymbol{k}) &= v f_{x,y}(\boldsymbol{k}), \quad (13)\\ b(\boldsymbol{k}) &= v_z f_z(\boldsymbol{k}). \quad (14) \end{aligned}$$

Here, we choose the chemical potential $\mu = 0.5$ eV, since the chemical potential measured from the surface Dirac point is 0.4∼0.5 eV according to Ref.41. We use the values of the parameters, c_2, m_0, m_2, v as given in Ref.50. On the other hand, for c_1, m_1, v_z, we choose the different values given in Ref.50, which involve the hopping along the c-axis. Since the parameterization performed in Ref.50 is based on the dispersion at around Γ-point, the difference of the dispersion near the zone boundary between the first principle calculation in Ref.50 and our tight-binding model is considerably large. However, the Fermi surface becomes a cylindrical one if we use the same parameters given in Ref.50 although the correct shape of the Fermi surface is an oval spherical one. Thus, we choose the values of c_1, m_1, v_0 as $c_1/c^2 = 0.024$, $m_1/c^2 = 0.216$, $v_z/c = 0.32$ (eV) to fit the energy dispersion for the Γ-Z direction obtained in Ref.50. These parameters give the oval spherical Fermi surface consistent with the first principle calculation. This parameterization is crucial since specific heat and spin susceptibility in actual $Cu_xBi_2Se_3$ can not be reproduced if we use a cylindrical Fermi surface. In addition, to obtain the topological superconductivity in three dimensions, the correct Fermi surface topology is needed .[5,6,48]

Next, we consider the pair potential. We assume that the pair potential is independent of momentum since the present material is not a strongly-correlated system.[48] In this case, these pair potentials are classified into four kinds of irreducible representation for D_{3d} point group. The matrix forms of the pairings Δ_1, Δ_2, Δ_3 and Δ_4 are shown in the first column of Table. I. Δ_1 and Δ_3 are spin-singlet intra-orbital pairings, whereas Δ_2 and Δ_4 are spin-triplet inter-orbit pairings in the orbital basis.

We diagonalize the BdG Hamiltonian Eq.(1). We obtain four branches of the bulk spectrum E_γ ($\gamma = 1, 2, 3, 4$) for each pairing,

$$\begin{aligned} E_1(\boldsymbol{k}) &= \sqrt{\xi^2(\boldsymbol{k}) + 2\sqrt{\eta^2(\boldsymbol{k})c^2(\boldsymbol{k}) + \zeta^2(\boldsymbol{k})\Delta^2}}, \quad (15)\\ E_2(\boldsymbol{k}) &= \sqrt{\xi^2(\boldsymbol{k}) - 2\sqrt{\eta^2(\boldsymbol{k})c^2(\boldsymbol{k}) + \zeta^2(\boldsymbol{k})\Delta^2}}, \quad (16)\\ E_3(\boldsymbol{k}) &= -\sqrt{\xi^2(\boldsymbol{k}) + 2\sqrt{\eta^2(\boldsymbol{k})c^2(\boldsymbol{k}) + \zeta^2(\boldsymbol{k})\Delta^2}}, \quad (17)\\ E_4(\boldsymbol{k}) &= -\sqrt{\xi^2(\boldsymbol{k}) - 2\sqrt{\eta^2(\boldsymbol{k})c^2(\boldsymbol{k}) + \zeta^2(\boldsymbol{k})\Delta^2}}, \quad (18) \end{aligned}$$

with

$$\begin{aligned} \eta^2(\boldsymbol{k}) &= m^2(\boldsymbol{k}) + a_x^2(\boldsymbol{k}) + a_y^2(\boldsymbol{k}) + b^2(\boldsymbol{k}), \quad (19)\\ \xi^2(\boldsymbol{k}) &= \eta^2(\boldsymbol{k}) + c^2(\boldsymbol{k}) + \Delta^2. \quad (20) \end{aligned}$$

The difference of energy gap structure in each pairing comes from $\zeta^2(\boldsymbol{k})$,

$$\begin{aligned} \Delta_1 : \zeta^2(\boldsymbol{k}) &= 0, \quad (21)\\ \Delta_2 : \zeta^2(\boldsymbol{k}) &= m^2(\boldsymbol{k}), \quad (22)\\ \Delta_3 : \zeta^2(\boldsymbol{k}) &= m^2(\boldsymbol{k}) + b^2(\boldsymbol{k}), \quad (23)\\ \Delta_4 : \zeta^2(\boldsymbol{k}) &= m^2(\boldsymbol{k}) + a_y^2(\boldsymbol{k}). \quad (24) \end{aligned}$$

Energy gap structure of Δ_1 is isotropic full gap, which is the same as the conventional BCS superconductors. In other cases, because of the presence of ζ, energy gap is modified from BCS gap structure. Δ_2 is anisotropic full gap pairing. In the case of Δ_3 and Δ_4, energy gap has point nodes. Point nodes for Δ_3 are on the poles. In the case of Δ_4, point nodes appear on the k_y-axis. Although, in general, Δ_4 is a linear combination of $\Delta\sigma_y s_x$ and $\Delta\sigma_y s_y$, we can choose $\Delta_4 = \sigma_y s_x$ without losing a generality. Energy gap of E_γ is influenced by the spin-orbit interaction v. To elucidate the role of the spin orbit interaction, we also consider the case of $v = 0$. In this case, E_γ for Δ_1 has a full gap, E_γs for Δ_2 and Δ_4 have line nodes on equator, and E_γ for Δ_3 is gapless.

III. SPECIFIC HEAT

In this section, we calculate the specific heat below T_c for each pairing symmetry. The specific heat is given by

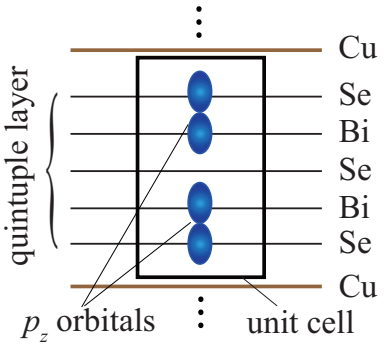

FIG. 1: (color online) Two p_z-orbitals in the quintuple layer of Bi_2Se_3.

pair potential	rep.	spin	orbital	energy gap
$\Delta_1 = \Delta$	A_{1g}	singlet	intra	isotropic full gap
				(isotropic full gap)
$\Delta_2 = \Delta\sigma_y s_z$	A_{1u}	triplet	inter	anisotropic full gap
				(line node on equator)
$\Delta_3 = \Delta\sigma_z$	A_{2u}	singlet	intra	point nodes at poles
				(gapless)
$\Delta_4 = \Delta\sigma_y s_x$	E_u	triplet	inter	point node on equator
				(line node on equator)

TABLE I: The irreducible representation, the spin state, the orbital state and the energy gap structure in each pairing symmetry. In the bracket we denote the gap structure for $v = 0$.

$$C_s = -\frac{2\beta}{N}\sum_{\boldsymbol{k}\gamma}\left(-\frac{\partial f(E_\gamma(\boldsymbol{k}))}{\partial E_\gamma(\boldsymbol{k})}\right)\left(E_\gamma^2(\boldsymbol{k}) + \frac{\beta}{2}\frac{\partial E_\gamma^2(\boldsymbol{k})}{\partial\beta}\right)$$
$$= -\frac{2\beta}{N}\sum_{\boldsymbol{k}\gamma}\left(-\frac{\partial f(E_\gamma(\boldsymbol{k}))}{\partial E_\gamma(\boldsymbol{k})}\right)$$
$$\times\left(E_\gamma^2(\boldsymbol{k}) + \beta E_\gamma(\boldsymbol{k})\frac{\partial\Delta}{\partial\beta}\frac{\partial E_\gamma(\boldsymbol{k})}{\partial\Delta}\right), \quad (25)$$

where N is the number of unit cells and β is $1/k_BT$ with the Boltzmann constant k_B and temperature T. We assume the temperature dependence of the pairing potential is the scaled BCS one, $\Delta(T) = (\alpha/\alpha_{\rm BCS})\Delta_{\rm BCS}(T)$. The magnitude of α gives the ratio of $\Delta(T=0)$ to T_c, i.e., $\alpha = \Delta(T=0)/(k_BT_c)$. This model is dubbed as α-model.[51] For $\Delta_{\rm BCS}(T)$, we use the following phenomenological form,[52]

$$\Delta_{\rm BCS}(T) = \alpha_{\rm BCS}k_BT_c\tanh\left(1.74\sqrt{\frac{T_c}{T}-1}\right), \quad (26)$$

with $\alpha_{\rm BCS} = 1.76$.

Since α is the material-dependent parameter and it often deviates from the BCS value $\alpha_{\rm BCS} = 1.76$, we use two different values. One is $\alpha = \alpha_{\rm BCS}$, and the other is $\alpha = \alpha_0$ where $C_s(T)/T$ at $T = 0.53T_c \equiv T_0$ becomes equal to that for the normal state $C_n(T)/T \simeq C_n(T_c)/T_c$ as observed in the specific heat measurement.[43]

A. Isotropic full gap Δ_1

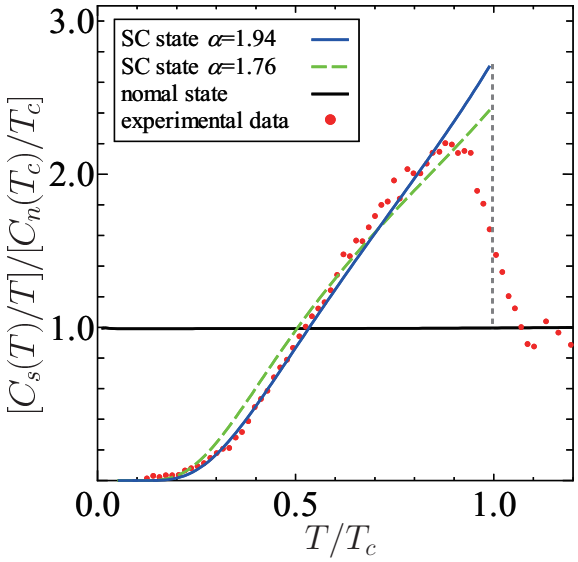

FIG. 2: (color online) Temperature dependence of specific heat for Δ_1 with $\alpha = 1.94$(blue solid line) and $\alpha = 1.76$(green dash line). Black solid line shows specific heat for nomal state. Red dotted circles show the experimental data by Ref.43

In Fig. 2, we show the temperature dependence of C_s for $\alpha = 1.76$ (green dash line) and $\alpha = \alpha_0 = 1.94$ (blue solid line). In the case of Δ_1, the energy spectrum is given by $E(\boldsymbol{k}) = \pm\sqrt{\varepsilon_\pm^2(\boldsymbol{k}) + \Delta^2}$, where $\varepsilon_\pm^2(\boldsymbol{k})$ is the dispersion of normal state. Therefore, the energy gap structure becomes isotropic s-wave one. Thus, the specific heat near $T = 0$ shows an exponential behavior. If we choose $\alpha = \alpha_{\rm BCS}$, T_0 and the magnitude of specific-heat jump are smaller than those of the experiment. To fit the experimental data, we choose $\alpha = \alpha_0 = 1.94$. Then, to satisfy the entropy balance relation,

$$\int_0^{T_c} dT\frac{C_s(T) - C_n(T)}{T} = 0, \quad (27)$$

the magnitude of the specific-heat jump at $\alpha = 1.94$ becomes larger than that for $\alpha = \alpha_{\rm BCS}$.

In the case of $\alpha = \alpha_0$, the magnitude of the specific heat jump and the line shape are similar to those of the experimental ones. We note that the analysis performed in Ref.43 is based on isotropic s-wave gap and therefore the obtained value of α_0 is almost the same. On the other hand, the value of α can be also estimated from the upper and the lower critical field in Ref.43. The estimated value

is $\alpha = 2.3 \equiv \alpha_c$. Therefore, the value of α_0 for Δ_1 deviates from that of α_c. However, if we add a small $\boldsymbol{k}$-dependent term allowed in A_{1g} representation to Δ_1, the magnitude of specific heat jump for $\alpha = \alpha_{\rm BCS}$ could be small and the values of α_0 becomes large, then, $\alpha_0 = 2.3$ might be obtained.

B. Anisotropic full gap Δ_2

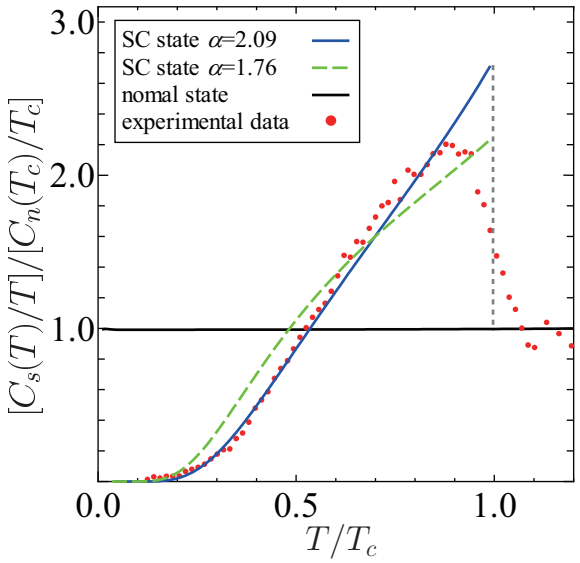

FIG. 3: (color online) Temperature dependence of specific heat for Δ_2 with $\alpha = 2.09$. The dotted circles show the experimental data by Ref.43

In Fig. 3, we show the temperature dependence of $C_s(T)$ for $\alpha = 1.76$ (green dash line) and $\alpha = \alpha_0 = 2.09$ (blue solid line). Since the energy gap structure is fully gapped, the exponential behavior appears near $T = 0$ as in the case of Δ_1. On the other hand, the magnitude of specific heat jump for $\alpha = \alpha_{\rm BCS}$ is smaller than that for Δ_1 owing to the anisotropy of the energy gap. Therefore, to reproduce the experimental data, we need larger value of α_0 compared with the case of Δ_1, $\alpha_0 = 2.09$. This value is closer to $\alpha_c = 2.3$ than that for Δ_1. The magnitude of the specific heat jump and the line shape for $\alpha = \alpha_0$ are similar to those of the experimental ones.

C. Point nodes at polar Δ_3

In the case of Δ_3, the energy dispersion has point nodes along k_z-axis. Thus, $C_s(T)/T$ has T^2-behavior near $T = 0$. The magnitude of the jump for $\alpha = \alpha_{\rm BCS}$ is the smallest among the four kinds of the pair potentials considered in this paper. This small jump is originated from the gapless nature of this pair potential. In the case of $v = 0$, the energy dispersion for Δ_3 is given by $E(\boldsymbol{k}) = \pm\sqrt{m^2(\boldsymbol{k}) + b^2(\boldsymbol{k})} \pm \sqrt{c(\boldsymbol{k})^2 + \Delta^2}$. This energy spectrum becomes gapless when $m^2(\boldsymbol{k}) + b^2(\boldsymbol{k}) = c(\boldsymbol{k})^2 + \Delta^2$. Parameters of STI satisfy the following relations.

$$m_0^2 - \mu^2 - \Delta^2 < 0, \tag{28}$$
$$m_1^2 - c_1^2 > 0, \tag{29}$$
$$m_2^2 - c_2^2 > 0. \tag{30}$$

In this case, the energy spectrum becomes gapless near the Fermi surface in any direction of $\boldsymbol{k}$. Thus, $C_s(T)/T$ with $v = 0$ is T-independent. In the presence of v, these gapless energy spectra still remain in the direction of k_z-axis and point nodes are formed since $a_{x,y}(\boldsymbol{k}) = 0$ in this direction. In the directions other than k_z, the energy gap is generated by the spin-orbit coupling v, but the gap is comparatively smaller than the other pairings. Therefore, the T-dependence of $C_s(T)/T$ for $\alpha = \alpha_{\rm BCS}$ remains relatively small. This is the reason why the specific heat jump is small for Δ_3 compared to other pair potentials. If we use $\alpha = \alpha_0 = 2.74$, we can adjust the specific heat jump similar to the experimental one and $[C_s(T_0)/T_0]/[C_n(T_c)/T_c]$ becomes equal to the unity. However, the line shape does not reproduce the experimental data. In addition, the value of α_0 is much larger than the experimental value $\alpha_c = 2.3$.

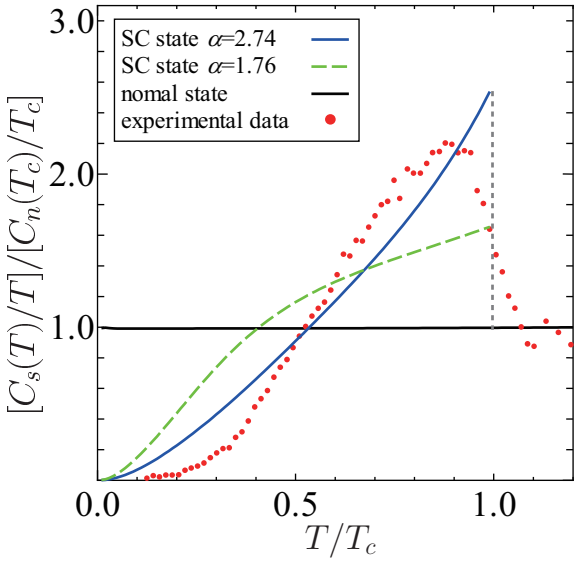

FIG. 4: (color online) Temperature dependence of specific heat for Δ_3 with $\alpha = 2.74$. The dotted circles show the experimental data by Ref.43

D. Point nodes on equator Δ_4

In the case of Δ_4, the energy spectrum has point nodes along k_y-axis. Therefore, $C_s(T)/T$ has T^2-behavior near $T = 0$ as in the case of Δ_3. However, in the case of

Δ_4, the energy spectrum does not become gapless even when v is absent. Thus, the coefficient of T^2 is smaller than the case of Δ_3 for $\alpha = \alpha_{\rm BCS}$, and the magnitude of the specific heat jump is larger than that for Δ_3. As a result, the line shape with $\alpha = \alpha_0 = 2.42$ is considerably close to the experimental one as compared with the case of Δ_3. The obtained value of $\alpha = 2.42$ is the most close to the experimental one, α_c, among the four kinds of the pairing symmetry considered in this paper.

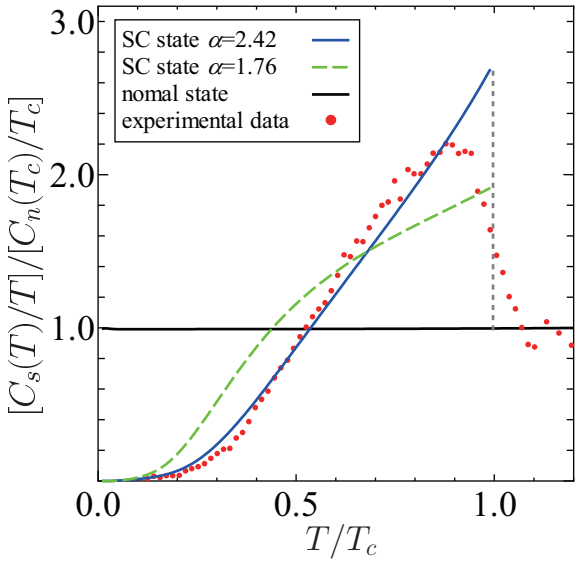

FIG. 5: (color online) Temperature dependence of specific heat for Δ_4 with $\alpha = 2.42$. The dotted circles show the experimental data by Ref.43

Here, we summarize the results of the specific heat. We have calculated the specific heat for $\alpha = \alpha_{\rm BCS}, \alpha_0$ in each pairing symmetry. For $\alpha = \alpha_0$, we obtain the line shapes similar to the experimental one in the cases of Δ_1, Δ_2, and Δ_4. The obtained values of α_0 are $\alpha = 1.94$, 2.09, 2.74, and 2.42 for Δ_1, Δ_2, Δ_3, and Δ_4, respectively. The values of α for Δ_2 and Δ_4 are closer to the experimental one ($\alpha_c = 2.3$), as compared with the other pair potentials.

IV. SPIN SUSCEPTIBILITY

From the temperature dependence of spin susceptibility, one can determine the spin structure of Cooper pairs. Namely, for a spin-singlet superconductor, the spin susceptibility along any direction decreases for $T < T_{\rm c}$ and vanishes at $T = 0$. On the other hand, for spin-triplet superconductor, only the spin susceptibility parallel to the direction of d-vector decreases and vanishes at $T = 0$, and the spin susceptibility perpendicular to d-vector is independent of T. However, the temperature dependence of spin susceptibility of a STI is not simple because spin-singlet and spin-triplet components can mix in the band basis due to the spin-orbit interaction depending on the pair potential.

pair potential	effects of SOI
$\Delta_1 = \Delta$	Van Vleck
$\Delta_2 = \Delta\sigma_y s_z$	Van Vleck rotation of d-vector
$\Delta_3 = \Delta\sigma_z$	Van Vleck induced spin-triplet
$\Delta_4 = \Delta\sigma_y s_x$	Van Vleck rotation of d-vector induced spin-singlet

TABLE II: Summary of spin susceptibility. Effects of spin-orbit interaction (SOI) is Van Vleck susceptibility, rotation of d-vector, and to induce spin-singlet and spin-triplet pair potentials.

Nevertheless, we show here that it is possible to determine spin structure of STI, even if spin-orbit interaction is present. The temperature dependences of spin susceptibility with each possible pairing are different from each other. For Δ_1, the spin susceptibility along any directions decreases as temperature decreases, since Δ_1 is a spin-singlet pair potential in the band basis. On the other hand, that along z-axis for Δ_3 is independent of temperature, although those along x- and y-axes decrease. Spin susceptibilities with Δ_2 and Δ_4 along the d-vector ($\boldsymbol{d} \parallel z$ for Δ_2 and $\boldsymbol{d} \parallel x$ for Δ_4) decrease. Those perpendicular to the d-vector are almost independent of temperature. The temperature dependences of spin susceptibility are summarized in Table III.

Now we comment on effects of spin-orbit interaction for spin susceptibility. There are three effects. The first one is Van Vleck susceptibility, which comes from inter-band (off-diagonal) matrix elements. Van Vleck susceptibility can appear in multiband systems with spin-orbit interaction. This leads to a non-zero value of spin susceptibility at $T = 0$ (See Appendix A 1). The second one is the rotation of d-vector by the unitary transformation from the orbital basis to the band basis. Then, the d-vector in band basis is not parallel to the Zeeman magnetic field, even when the d-vector in the orbital basis is. This also induces a non-zero value of spin susceptibility at $T = 0$. Additionally, the spin susceptibility perpendicular to d-vector in the orbital basis also decreases slightly for $T < T_{\rm c}$. This behavior shows up in the case of Δ_2 and Δ_4. The third one is a generation of spin-singlet and spin-triplet pair potentials in the band basis from spin-triplet and spin-singlet ones in the orbital basis, respectively. In the following sections, we shall discuss the temperature dependence of the spin susceptibility in each pairing.

A. Kubo formula for spin susceptibility

First, we give the Zeeman term in a STI and Kubo formula for spin susceptibility. The Zeeman term $H_{\rm Z}(\boldsymbol{k})$ is given by

$$H_{\rm Z}(\boldsymbol{k}) = \sum_{i=x,y,z} \sum_{\mu=0,x,y,z} h_i \mu_{\rm B} \frac{g_{i\mu}}{2} s_i \sigma_\mu, \tag{31}$$

where $\mu_{\rm B}$ is Bohr magneton, h_i is the i-th component of Zeeman field, $g_{i\mu}$ is g-factor of the parent topological insulator, and σ_0 is 2×2 identity matrix in the orbital space. The spin susceptibility along i-axis is given by the Kubo formula:

$$\chi_i = -\mu_{\rm B}^2 \lim_{\boldsymbol{q}\to 0} \frac{1}{V} \sum_{\boldsymbol{k}\alpha\beta\mu} \frac{f(E_\alpha(\boldsymbol{k})) - f(E_\beta(\boldsymbol{k}+\boldsymbol{q}))}{E_\alpha(\boldsymbol{k}) - E_\beta(\boldsymbol{k}+\boldsymbol{q}) + i0} \times \langle\alpha|s_i|\beta\rangle\langle\beta|\frac{g_{i\mu}}{2} s_i\sigma_\mu|\alpha\rangle. \tag{32}$$

In actual calculation, we set $g_{i\mu}$ to be that of Bi_2Se_3:[50] $g_{x0} = g_{y0} = -8.92, g_{z0} = -21.3, g_{xx} = g_{yx} = 0.68, g_{zx} = -29.5$. The other g-factors are chosen to be zero. Temperature dependence of Δ is same as that used in the calculation of specific heat with $\alpha = 2.3$.

B. Spin structure in the band basis

In the band basis, spin-singlet and spin-triplet pair potentials can mix each other because of spin-orbit interaction . Due to this, it is rather difficult to understand the temperature dependence of spin susceptibility. In order to clarify the spin structures of pair potentials, it is necessary to introduce the band basis where the normal part of Hamiltonian is diagonalized. First, we diagonalize the Hamiltonian $H_0(\boldsymbol{k})$ of the normal state as

$$H_0(\boldsymbol{k})\boldsymbol{u}_\gamma(\boldsymbol{k}) = \epsilon_\gamma(\boldsymbol{k})\boldsymbol{u}_\gamma(\boldsymbol{k}), \tag{33}$$

with band index γ. By using the unitary matrix $U(\boldsymbol{k})$ given by $U(\boldsymbol{k}) = (\boldsymbol{u}_1(\boldsymbol{k}), \boldsymbol{u}_2(\boldsymbol{k}), \cdots)$, the pair potential $\hat{\Delta} = \sum_\mu d_\mu s_\mu$ is transformed as

$$\sum_\mu d_\mu s_\mu \to U^\dagger(\boldsymbol{k}) \sum_\mu d_\mu s_\mu U(\boldsymbol{k}) = \sum_\mu \tilde{d}_\mu(\boldsymbol{k}) s_\mu. \tag{34}$$

$\tilde{d}_0(\boldsymbol{k})$ and $\tilde{\boldsymbol{d}}(\boldsymbol{k})$ denote spin singlet-component of pair potential and d-vector of spin-triplet component of pair potentials in the band basis, respectively. It is noted that s_μ does not change by this unitary transformation in inversion-symmetric systems. The corresponding Hamiltonian is expressed as

$$U^\dagger(\boldsymbol{k})H(\boldsymbol{k})U(\boldsymbol{k}) = {\rm diag}(\epsilon_1(\boldsymbol{k}) - \mu, \epsilon_2(\boldsymbol{k}) - \mu, \cdots)\tau_z + \sum_\mu \tilde{d}_\mu(\boldsymbol{k}) s_\mu \tau_x. \tag{35}$$

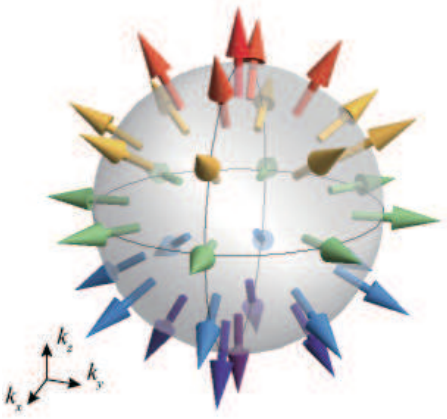

FIG. 6: (color online) Vector field plot of the conduction-band component of $\tilde{\boldsymbol{d}}(\boldsymbol{k})$ for Δ_2 [(1,1)-component of Eq. (37)].

In the following, we show the d-vectors in the band basis in the lowest order of $\boldsymbol{k}$. The detailed derivation of $\tilde{d}_\mu(\boldsymbol{k})$ is shown in Appendix. In the case of Δ_1, $\tilde{d}_\mu(\boldsymbol{k})$ is the same as in the orbital basis: $d_0(\boldsymbol{k}) = \Delta, \boldsymbol{d}(\boldsymbol{k}) = \boldsymbol{0}$. For other cases, we have

Δ_2 :

$$\tilde{d}_0(\boldsymbol{k}) = 0, \tag{36}$$

$$\tilde{\boldsymbol{d}}(\boldsymbol{k}) = \Delta\left(\frac{vk_x}{m_0}, \frac{vk_y}{m_0}, \frac{v_z k_z}{|m_0|}\tilde{\sigma}_z - {\rm sgn}(m_0)\tilde{\sigma}_y\right), \tag{37}$$

Δ_3 :

$$\tilde{d}_0(\boldsymbol{k}) = \Delta\tilde{\sigma}_x, \tag{38}$$

$$\tilde{\boldsymbol{d}}(\boldsymbol{k}) = \Delta\tilde{\sigma}_z\left(-\frac{vk_y}{|m_0|}, \frac{vk_x}{|m_0|}, 0\right), \tag{39}$$

Δ_4 :

$$\tilde{d}_0(\boldsymbol{k}) = \Delta\frac{vk_y}{m_0}\frac{v_z k_z}{m_0}\tilde{\sigma}_x, \tag{40}$$

$$\tilde{\boldsymbol{d}}(\boldsymbol{k}) = \Delta\left(\frac{v_z k_z}{|m_0|}\tilde{\sigma}_z - \tilde{\sigma}_y, 0, -\frac{vk_x}{m_0}\right), \tag{41}$$

Here, $\tilde{\sigma}_i$ is Pauli matrix denoting band index, i.e., $\tilde{\sigma}_z = 1$ for the conduction band, $\tilde{\sigma}_z = -1$ for the valence band. To illustrate the $\tilde{d}(\boldsymbol{k})$ of Eq.(37) in the conduction (valence) band, we plot the $(1,1)$-component ($(2,2)$-component) of the $\tilde{d}$ vector in Fig.6 (Fig.7). Those of Eqs. (39) and (41) are also shown in Figs. 8, 9, 10, and 11, respectively. $\tilde{d}_\mu(\boldsymbol{k})$ is useful to understand the temperature dependence of χ_i, as we will see in the following.

C. Isotropic full-gap Δ_1: Van Vleck susceptibility

Fig. 12 shows the temperature dependence of χ_i with Δ_1 for $v = 3.33$ eV Å and $v = 0$, respectively, where

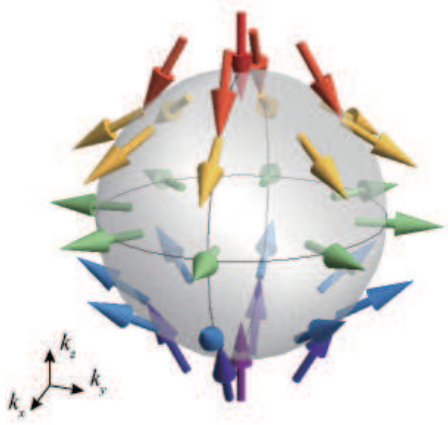

FIG. 7: (color online) Vector field plot of the valence-band component of $\tilde{\boldsymbol{d}}(\boldsymbol{k})$ for Δ_2 [(2,2)-component of Eq. (37)].

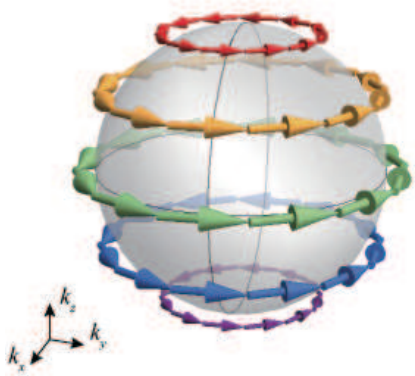

FIG. 8: (color online) Vector field plot of the conduction-band component of $\tilde{\boldsymbol{d}}(\boldsymbol{k})$ for Δ_3 [(1,1)-component of Eq. (39)].

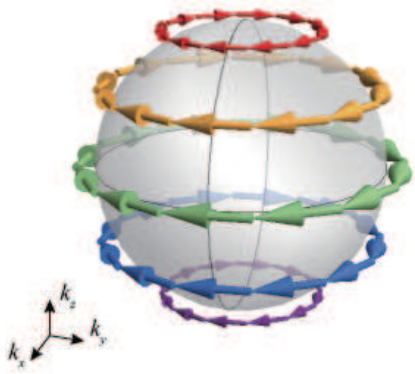

FIG. 9: (color online) Vector field plot of the valence-band component of $\tilde{\boldsymbol{d}}(\boldsymbol{k})$ for Δ_3 [(2,2)-component of Eq. (39)].

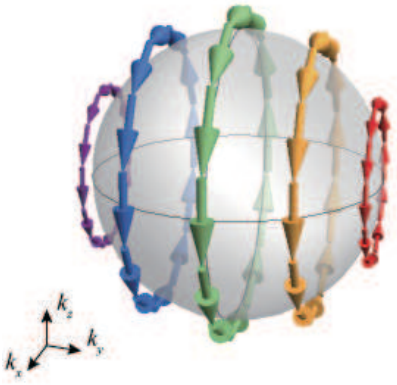

FIG. 10: (color online) Vector field plot of the conduction-band component of $\tilde{\boldsymbol{d}}(\boldsymbol{k})$ for Δ_4 [(1,1)-component of Eq. (41)].

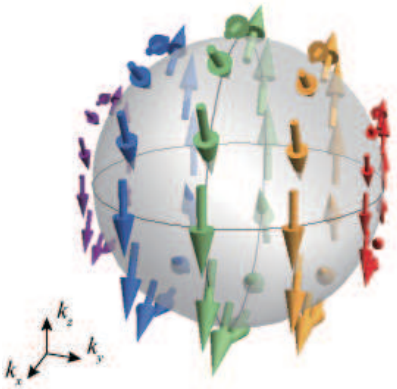

FIG. 11: (color online) Vector field plot of the valence-band component of $\tilde{\boldsymbol{d}}(\boldsymbol{k})$ for Δ_4 [(2,2)-component of Eq. (41)].

v corresponds to the strength of spin-orbit interaction. STI with Δ_1 is a full-gapped superconductor, therefore resulting χ_x, χ_y, and χ_z decrease exponentially for $T < T_c$ both for $v = 0$ and $v = 3.33$ eV Å. In the case of $v = 0$, all χ_is vanish at $T = 0$ as shown by the dashed lines in Fig. 12. On the other hand, in the presence of v, all χ_is remain to be a finite value at $T = 0$ (the solid line in Fig. 12) due to the Van Vleck susceptibility,[53] which is allowed in a multi-band system with spin-orbit interaction. Actually, χ_z at $T = 0$ is proportional to v^2 (See Appendix[A 1]). It is noted that the value of χ_z is larger than those of χ_x and χ_y in the normal state, because of the anisotropy of the energy band.

D. Anisotropic full-gap Δ_2: Rotation of d-vector

The d-vector in STI with Δ_2 is parallel to the z-axis in the orbital basis. In the absence of spin orbit interaction, the d-vector for Δ_2 in band basis is also parallel to the z-axis as shown in Eq.(37). Consequently, only χ_z

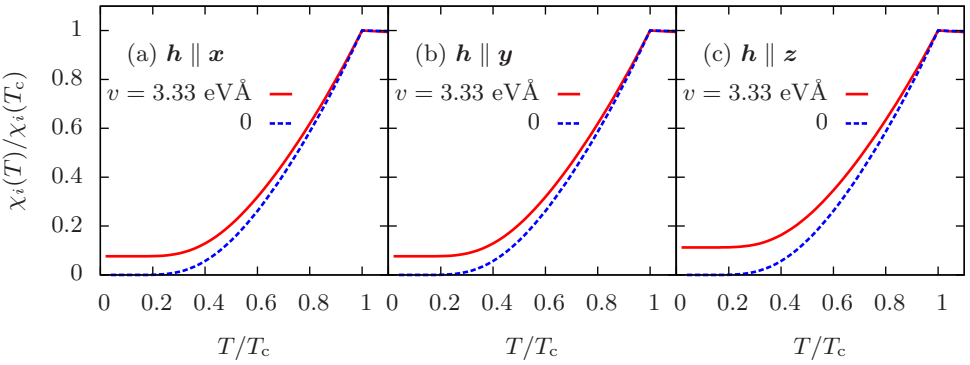

FIG. 12: (color online) Tesmperature dependences of spin susceptibilities χ_x (a), χ_y (b), and χ_z (c) of STI with Δ_1 in the presence ($v = 3.33$ eV Å, solid line) and absence ($v = 0$, dashed line) of spin-orbit interaction. The value of χ_i is normalized by that in the normal state, which is given by $\chi_x(T_c) = \chi_y(T_c) = 0.309\chi_z(T_c)$ for $v = 3.33$ eV Å and $\chi_x(T_c) = \chi_y(T_c) = 0.210\chi_z(T_c)$ for $v = 0$.

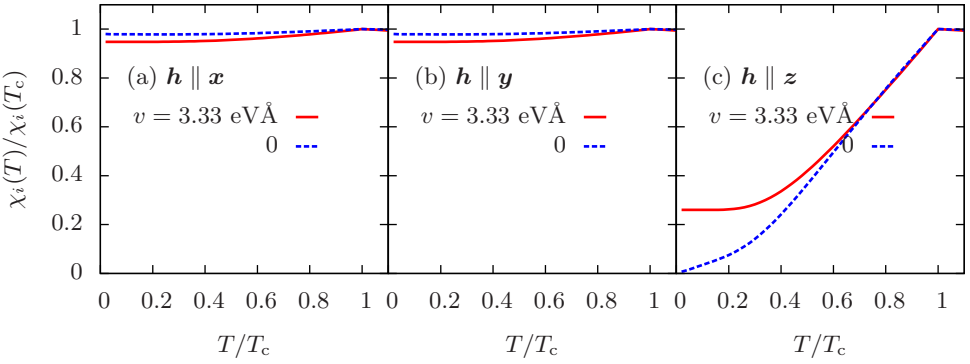

FIG. 13: (color online) Temperature dependences of spin susceptibilities of STI with Δ_2.

decreases and vanishes at $T = 0$, and χ_x, χ_y are independent of T, as shown in Fig. 13. In the low temperature, χ_z is proportional to T since STI with Δ_2 has a line node on the equator for $v = 0$, as discussed in Sec. II. In the presence of v, χ_z decreases exponentially for $T < T_c$, as denoted by the solid line in Fig. 13(c). In addition to this, χ_x and χ_y slightly decrease [the solid lines in Fig. 13(a)(b)] since the d-vector is rotated so that d_x and d_y-components are induced in the band basis. χ_z at $T = 0$ takes a finite value by the following two reasons. First, $\tilde{\boldsymbol{d}}(\boldsymbol{k})$ is not parallel to the z-axis. Second, Van Vleck susceptibility arises, as in the case of Δ_1.

E. Point node on poles Δ_3: Induced spin-triplet pair potential

For v=0, all χ_i's of STI with Δ_3 are independent of T, as denoted by the dashed line in Fig. 14, since the energy spectrum is gapless (Sec. III C). On the other hand, for $v = 3.33$ eVÅ, χ_x and χ_y decrease down to $\chi_i(T = 0)/\chi_i(T_c) \sim 0.4$ at $T = 0$ [the solid lines in Fig. 14(a)(b)], while χ_z is independent of T [the solid line in Fig. 13(c)]. This behavior is understood from the induced spin-triplet component $\tilde{\boldsymbol{d}}(\boldsymbol{k})$ in Eq. (39) due to the spin-orbit interaction. The induced d-vector $\tilde{\boldsymbol{d}}(\boldsymbol{k})$ is parallel to the xy-plane, as shown in Figs. 8 and 9, consequently the χ_z becomes independent of T. Moreover, χ_x and χ_y take a finite value at $T = 0$, due to the Van Vleck susceptibility. The similar result has been obtained in the bilayer system.[53]

F. Point nodes on equator Δ_4: Rotation of d-vector and induced spin-singlet pair potential

For $v = 0$, due to $\tilde{\boldsymbol{d}}(\boldsymbol{k}) \parallel \boldsymbol{x}$ in the band basis, only χ_x decreases for $T < T_c$ and vanishes at $T = 0$ [the dashed line Fig. 15(a)]. In the low temperature, χ_x is proportional to T since the energy spectrum has a line node on the equator (See Sec. II). For $v = 3.33$ eVÅ, χ_x decreases with T and is proportional to T^2 in the low temperature, except for the residual value at $T = 0$. This residual spin susceptibility comes from the rotated d-vector and Van Vleck susceptibility, due to spin-orbit interaction. χ_z slightly decreases for $T < T_c$ since $\tilde{d}_z(\boldsymbol{k})$ is present. On the other hand, $\tilde{d}_y(\boldsymbol{k})$ vanishes up to the first order of $\boldsymbol{k}$ [Eq. (41) and Figs. 10, 11], and thus χ_y is almost independent of T [the solid line in Fig. 15(b)].

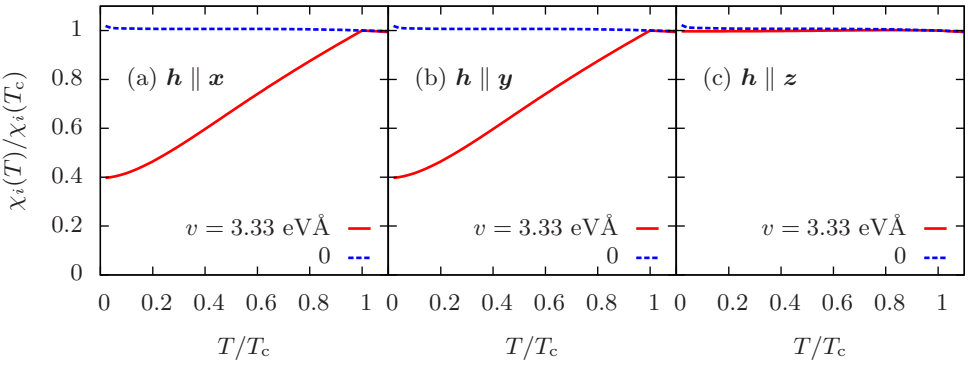

FIG. 14: Temperature dependences of spin susceptibilities of STI with Δ_3.

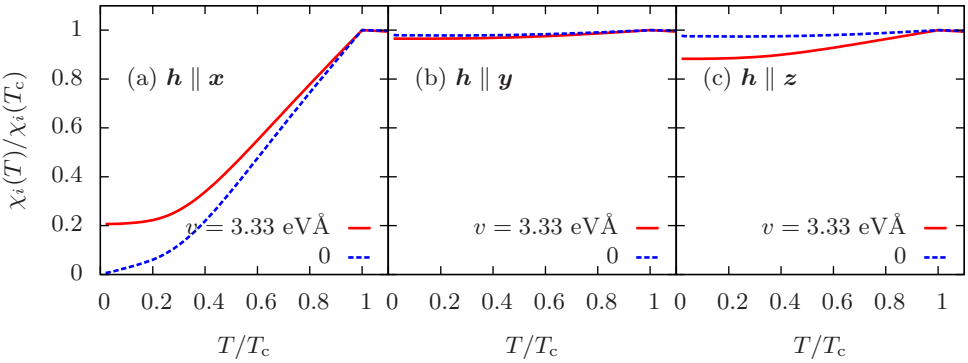

FIG. 15: (color online) Temperature dependences of spin susceptibilities of STI with Δ_4.

V. DISCUSSION AND SUMMARY

In this paper, we have calculated the temperature dependence of the specific heat and the spin susceptibility. The temperature dependences of the specific heat are similar among three of four possible pair potentials. On the other hand, wide varieties of temperature dependence appear in spin susceptibility depending on the direction of the applied magnetic field. These results are summarized in Table III.

Finally, we compare the obtained results and the experimental ones. From the temperature dependence of the specific heat, Δ_1, Δ_2, and Δ_4 are almost consistent with the experimental result. On the other hand, recent tunneling spectroscopy for the (111) surface of $Cu_xBi_2Se_3$ has shown a pronounced ZBCP.[33] From the theoretical calculation, the ZBCP due to ABSs is generated on the (111) surface only for the case with Δ_2 and Δ_4.[29,33] Based on these background, promising pair potentials are Δ_2 and Δ_4. In the light of the obtained spin susceptibility in this paper, we conclude that it is possible to distinguish between Δ_2 and Δ_4 by measuring the temperature dependence of in-plane and out-of-plane Knight shifts.

pairing potential	specific heat C_s	Andreev bound state	spin susceptibility χ_x	χ_y	χ_z
$\Delta_1 = \Delta\sigma$	yes	no	↙	↙	↙
$\Delta_2 = \Delta\sigma_y s_z$	yes	yes	−	−	↙
$\Delta_3 = \Delta\sigma_z$	no	no	↙	↙	−
$\Delta_4 = \Delta\sigma_y s_x$	yes	yes	↙	−	−

TABLE III: [First column] Possible pairing symmetry of a STI. [Second column] Comparison of line shape between our results and the experimental one.[43] [Third column] Presence or absence of ZBCP due to ABSs.[29,33] [Fourth column] The temperature dependence of χ_x, χ_y, and χ_z. ↙ denotes decreasing of χ_i with decreasing the temperature. − denotes that χ_i is almost independent of the temperature.

VI. ACKNOWLEDGEMENTS

We gratefully thanks to M. Kriener, K Segawa, Z. Ren, S. Sasaki and Y. Ando for variable discussions and providing the experimental data. We gratefully acknowledge S. Onari for valuable discussions. This work was supported in part by a Grant-in Aid for Scientific Research from MEXT of Japan, "Topological Quantum Phenomena,h Grants No. 22103005, No. 20654030 and No. 22540383

Appendix A: Effects of spin-orbit interaction

1. Van Vleck susceptibility for Δ_1

Here, we derive Van Vleck susceptibility, which gives a finite value of the spin susceptibility at $T = 0$. We focus on a STI with Δ_1, based on the Hamiltonian in the continuum limit as

$$H(\boldsymbol{k}) = [c(\boldsymbol{k}) + m(\boldsymbol{k})\sigma_x + v_z k_z \sigma_y + v k_\parallel h_s(\boldsymbol{k})\sigma_z]\tau_z + \Delta\tau_x. \tag{A1}$$

First, we diagonalize spin-part: $h_s(\boldsymbol{k}) = (\boldsymbol{k}\times\boldsymbol{s})_z/k_\parallel$, where $k_\parallel = |\boldsymbol{k}_\parallel| = (k_x^2+k_y^2)^{1/2}$. The eigenvalue $\tilde{s}$ of h_s is given by $\tilde{s} = \pm 1$. The corresponding eigenvector is given by

$$|\tilde{s}\rangle = \frac{1}{\sqrt{2}}\begin{pmatrix} 1 \\ \tilde{s}e^{i\varphi_{\boldsymbol{k}}}\end{pmatrix}, \tag{A2}$$

with $\sin\varphi_{\boldsymbol{k}} = k_x/k_\parallel$ and $\cos\varphi_{\boldsymbol{k}} = -k_y/k_\parallel$.

Next, we diagonalize the normal part: $H_{0\tilde{s}}(\boldsymbol{k}) = m(\boldsymbol{k})\sigma_x + v_z k_z\sigma_y + \tilde{s}vk_\parallel\sigma_z$. The eigenvalue of $H_{0\tilde{s}}(\boldsymbol{k})$ is given by $\tilde{\sigma}\eta(\boldsymbol{k}) + c(\boldsymbol{k})$ with

$$\eta(\boldsymbol{k}) = \sqrt{m^2(\boldsymbol{k}) + v_z^2 k_z^2 + v^2 k_\parallel^2}, \tag{A3}$$

and $\tilde{\sigma} = \pm 1$ being band index. The corresponding eigenvector $|\tilde{s}\tilde{\sigma}\rangle$ of $H_{0\tilde{s}}(\boldsymbol{k})$ is given by

$$|\pm,\pm\rangle = \begin{pmatrix} \cos p_{\boldsymbol{k}}/2 \\ \pm e^{iq_{\boldsymbol{k}}}\sin p_{\boldsymbol{k}}/2\end{pmatrix}, \tag{A4}$$

$$|\pm,\mp\rangle = \begin{pmatrix} \sin p_{\boldsymbol{k}}/2 \\ \mp e^{iq_{\boldsymbol{k}}}\cos p_{\boldsymbol{k}}/2\end{pmatrix}, \tag{A5}$$

with

$$\cos p_{\boldsymbol{k}} = vk_\parallel/\eta(\boldsymbol{k}), \tag{A6}$$

$$\sin p_{\boldsymbol{k}} = \sqrt{m^2(\boldsymbol{k}) + v_z^2 k_z^2}/\eta(\boldsymbol{k}), \tag{A7}$$

$$\cos q_{\boldsymbol{k}} = m(\boldsymbol{k})/\sqrt{m^2(\boldsymbol{k}) + v_z^2 k_z^2}, \tag{A8}$$

$$\sin q_{\boldsymbol{k}} = v_z k_z/\sqrt{m^2(\boldsymbol{k}) + v_z^2 k_z^2}. \tag{A9}$$

In the band basis, the original Hamiltonian is rewritten as

$$H_{\tilde{s}\tilde{\sigma}}(\boldsymbol{k}) = [\tilde{\sigma}\eta(\boldsymbol{k}) + c(\boldsymbol{k})]\tau_z + \Delta\tau_x. \tag{A10}$$

The energy eigenvalue of $H_{\tilde{s}\tilde{\sigma}}(\boldsymbol{k})$ is given by $\tau E_{\tilde{\sigma}}(\boldsymbol{k})$ with

$$E_{\tilde{\sigma}}(\boldsymbol{k}) = \sqrt{[\tilde{\sigma}\eta(\boldsymbol{k}) + c(\boldsymbol{k})]^2 + \Delta^2}, \tag{A11}$$

and $\tau = \pm 1$. The corresponding eigenvector $|\tilde{s}\tilde{\sigma}\tau\rangle$ is given by

$$|\tilde{s},\tilde{\sigma},+\rangle = \begin{pmatrix} \cos P_{\boldsymbol{k}\tilde{\sigma}}/2 \\ \sin P_{\boldsymbol{k}\tilde{\sigma}}/2\end{pmatrix}, \tag{A12}$$

$$|\tilde{s},\tilde{\sigma},-\rangle = \begin{pmatrix} \sin P_{\boldsymbol{k}\tilde{\sigma}}/2 \\ -\cos P_{\boldsymbol{k}\tilde{\sigma}}/2\end{pmatrix}, \tag{A13}$$

with $\cos P_{\boldsymbol{k}\tilde{\sigma}} = [\tilde{\sigma}\eta(\boldsymbol{k}) + c(\boldsymbol{k})]/E_{\tilde{\sigma}}(\boldsymbol{k})$.

For a full-gapped system, spin susceptibility at $T = 0$ is given by

$$\chi_i = \frac{2\mu_{\rm B}^2}{N}\sum_{\boldsymbol{k}\tilde{s}\tilde{s}'\tilde{\sigma}\tilde{\sigma}'}\frac{|\langle\tilde{s}|s_i|\tilde{s}'\rangle\langle\tilde{s},\tilde{\sigma}|\tilde{s}',\tilde{\sigma}'\rangle\langle\tilde{s},\tilde{\sigma},+|\tilde{s}',\tilde{\sigma}',-\rangle|^2}{E_{\tilde{\sigma}}(\boldsymbol{k}) + E_{\tilde{\sigma}'}(\boldsymbol{k})}. \tag{A14}$$

For simplicity, we assume that all the g-factors are equal to two, and we concentrate on χ_z. The matrix element in the above expression is estimated as follows.

$$\langle\tilde{s}|s_z|\tilde{s}'\rangle = 1 - \delta_{\tilde{s}\tilde{s}'}, \tag{A15}$$

$$\langle\tilde{s},\pm|-\tilde{s},\mp\rangle = \pm\cos p_{\boldsymbol{k}}, \tag{A16}$$

$$\langle\tilde{s},\tilde{\sigma},+|-\tilde{s},\tilde{\sigma}',-\rangle = \sin\frac{P_{\boldsymbol{k}\tilde{\sigma}'} - P_{\boldsymbol{k}\tilde{\sigma}}}{2}. \tag{A17}$$

From the above equations, only the Van Vleck term, which comes from the off-diagonal term of $\tilde{s}\neq\tilde{s}'$, $\tilde{\sigma}\neq\tilde{\sigma}'$, and $\tau\neq\tau'$, can be nonzero as

$$\chi_z = \frac{8\mu_{\rm B}^2}{N}\sum_{\boldsymbol{k}}\frac{1}{E_+(\boldsymbol{k}) + E_-(\boldsymbol{k})}\frac{v^2k_\parallel^2}{\eta^2(\boldsymbol{k})}\sin^2\frac{P_{\boldsymbol{k}+} - P_{\boldsymbol{k}-}}{2}. \tag{A18}$$

One can verify $\chi_z \to 0$ at $v \to 0$ from the above expression. Spin susceptibility at $T = 0$ in STI with Δ_1 stems from Van Vleck component due to the spin-orbit coupling v.

2. Rotation of d-vector for Δ_2

Here, we derive d-vector for Δ_2 in the band basis. The following relation is useful:

$$\begin{aligned}\langle\tilde{s},\tilde{\sigma}|\sigma_y|\tilde{s}',\tilde{\sigma}'\rangle = \big[&\delta_{\tilde{s}\tilde{s}'}\,(\tilde{\sigma}_z\sin p_{\boldsymbol{k}}\sin q_{\boldsymbol{k}} - \tilde{\sigma}_y\cos q_{\boldsymbol{k}}) \\ &- (\tilde{s}_z)_{\tilde{s}\tilde{s}'}\tilde{\sigma}_x\cos p_{\boldsymbol{k}}\sin q_{\boldsymbol{k}} \\ &+ (\tilde{s}_x)_{\tilde{s}\tilde{s}'}\,(\tilde{\sigma}_z\sin q_{\boldsymbol{k}} - \tilde{\sigma}_y\sin p_{\boldsymbol{k}}\cos q_{\boldsymbol{k}}) \\ &+ (\tilde{s}_y)_{\tilde{s}\tilde{s}'}\sigma_0\cos p_{\boldsymbol{k}}\cos q_{\boldsymbol{k}}\big]_{\tilde{\sigma}\tilde{\sigma}'}.\end{aligned} \tag{A19}$$

The above expression is derived with the use of Eqs. (A4) and (A5). The pair potential Δ_2 is represented in the band basis:

$$\begin{aligned}\Delta\sigma_y s_z = \Delta(&\sin q_{\boldsymbol{k}}\tilde{\sigma}_z - \cos q_{\boldsymbol{k}}\sin p_{\boldsymbol{k}}\tilde{\sigma}_y)\tilde{s}_x \\ &+ \Delta\cos q_{\boldsymbol{k}}\frac{vk_\parallel}{\eta(\boldsymbol{k})}\tilde{s}_y,\end{aligned} \tag{A20}$$

where $\tilde{s}_i$ is Pauli matrix in the spin-helicity space. Here, the relation between $\boldsymbol{s}$ and $\tilde{\boldsymbol{s}}$ is as follows.

$$\langle\tilde{s}|s_z|\tilde{s}'\rangle = 1 - \delta_{\tilde{s}\tilde{s}'} = (\tilde{s}_x)_{\tilde{s}\tilde{s}'} \tag{A21}$$

$$\langle\tilde{s}|s_x|\tilde{s}'\rangle = (\tilde{s}_y)_{\tilde{s}\tilde{s}'}\sin\varphi_{\boldsymbol{k}} + (\tilde{s}_z)_{\tilde{s}\tilde{s}'}\cos\varphi_{\boldsymbol{k}}, \tag{A22}$$

$$\langle\tilde{s}|s_y|\tilde{s}'\rangle = (\tilde{s}_z)_{\tilde{s}\tilde{s}'}\sin\varphi_{\boldsymbol{k}} - (\tilde{s}_y)_{\tilde{s}\tilde{s}'}\cos\varphi_{\boldsymbol{k}}, \tag{A23}$$

or equivalently,

$$\tilde{s}_x = s_z, \tag{A24}$$

$$\tilde{s}_y = s_x \sin\varphi_{\boldsymbol{k}} - s_y \cos\varphi_{\boldsymbol{k}} = \frac{\boldsymbol{k}_\parallel \cdot \boldsymbol{s}}{k_\parallel}, \tag{A25}$$

$$\tilde{s}_z = s_x \cos\varphi_{\boldsymbol{k}} + s_y \sin\varphi_{\boldsymbol{k}} = \frac{(\boldsymbol{k}\times\boldsymbol{s})_z}{k_\parallel}. \tag{A26}$$

Consequently, the d-vector for Δ_2 in the band basis is obtained as

$$\tilde{d}_x(\boldsymbol{k}) = \Delta\cos q_{\boldsymbol{k}} \frac{vk_x}{\eta(\boldsymbol{k})}, \tag{A27}$$

$$\tilde{d}_y(\boldsymbol{k}) = \Delta\cos q_{\boldsymbol{k}} \frac{vk_y}{\eta(\boldsymbol{k})}, \tag{A28}$$

$$\tilde{d}_z(\boldsymbol{k}) = \Delta(\sin q_{\boldsymbol{k}}\tilde{\sigma}_z - \cos q_{\boldsymbol{k}} \sin p_{\boldsymbol{k}}\tilde{\sigma}_y). \tag{A29}$$

It is noted that the spin in the above expression is represented in the original spin space ($\boldsymbol{s}$) not in the spin-helicity space ($\tilde{\boldsymbol{s}}$). For STI with Δ_2, spin-orbit interaction takes a role to rotate d-vector in the band basis. In the case of $v = 0$, due to $\tilde{\boldsymbol{d}}(\boldsymbol{k}) \parallel \boldsymbol{z}$, only χ_z decreases for $T < T_{\rm c}$. In the case of $v \neq 0$, $\tilde{d}_x(\boldsymbol{k})$ and $\tilde{d}_y(\boldsymbol{k})$ (proportional to v) are present, and χ_x and χ_y also decreases slightly for $T < T_{\rm c}$.

3. Induced spin-triplet pair for Δ_3

In the following, we show that a spin-triplet pair is induced for Δ_3 in the band basis. As in Appendix A 2, we derive $\tilde{\boldsymbol{d}}(\boldsymbol{k})$ for $\Delta_3 = \Delta\sigma_z$. By using Eqs. (A4) and (A5), the matrix elements of σ_z are obtained as

$$\langle\tilde{s},\tilde{\sigma}|\sigma_z|\tilde{s},\tilde{\sigma}'\rangle = (\tilde{s}\tilde{\sigma}_z\cos p_{\boldsymbol{k}} + \tilde{\sigma}_x \sin p_{\boldsymbol{k}})_{\tilde{\sigma}\tilde{\sigma}'}\,. \tag{A30}$$

Therefore, σ_z is expressed in the band basis as

$$\sigma_z = \sin p_{\boldsymbol{k}}\tilde{\sigma}_x + \frac{v(k_x s_y - k_y s_x)}{\eta(\boldsymbol{k})}\tilde{\sigma}_z. \tag{A31}$$

This is derived with the help of Eq. (A26). As a result, $\tilde{d}_0(\boldsymbol{k})$ and $\tilde{\boldsymbol{d}}(\boldsymbol{k})$ are given by

$$\tilde{d}_0(\boldsymbol{k}) = \Delta\sin p_{\boldsymbol{k}}\tilde{\sigma}_x, \tag{A32}$$

$$\tilde{\boldsymbol{d}}(\boldsymbol{k}) = \frac{v\Delta}{\eta(\boldsymbol{k})}\tilde{\sigma}_z(-k_y, k_x, 0). \tag{A33}$$

which implies that a spin-triplet pair is induced in the band basis. Note that $\tilde{\boldsymbol{d}}(\boldsymbol{k}) \perp \boldsymbol{z}$. This is the reason why almost only χ_z in STI with Δ_3 decreases with temperature.

4. Induced spin-singlet pair and rotation of d-vector for Δ_4

In this subsection, we derive d-vector for $\Delta_4 = \sigma_y s_x$, and show that a spin-singlet pair is induced and the d-vector is rotated in the band basis. From the matrix elements of σ_y [Eq. (A19)] and of s_x [Eq. (A22)], the pair potential Δ_4 in the band basis is represented as follows,

$$\begin{aligned}\Delta\sigma_y s_x = {}& \Delta\frac{vk_y}{\eta(\boldsymbol{k})}\sin q_{\boldsymbol{k}}\tilde{\sigma}_x - \Delta\frac{vk_x}{\eta(\boldsymbol{k})}\cos q_{\boldsymbol{k}}\tilde{s}_x \\ & + \Delta\frac{k_x}{k_\parallel}(\sin q_{\boldsymbol{k}}\tilde{\sigma}_z - \sin p_{\boldsymbol{k}}\cos q_{\boldsymbol{k}}\tilde{\sigma}_y)\tilde{s}_y \\ & - \Delta\frac{k_y}{k_\parallel}(\sin p_{\boldsymbol{k}}\sin q_{\boldsymbol{k}}\tilde{\sigma}_z - \cos q_{\boldsymbol{k}}\tilde{\sigma}_y)\tilde{s}_z. \end{aligned}\tag{A34}$$

Using Eqs. (A24), (A25), and (A26), the d-vector for Δ_4 in the band basis is obtained as

$$\tilde{d}_0(\boldsymbol{k}) = \Delta\frac{vk_y}{\eta(\boldsymbol{k})}\sin q_{\boldsymbol{k}}\tilde{\sigma}_x, \tag{A35}$$

$$\begin{aligned}\tilde{d}_x(\boldsymbol{k}) = \Delta\Bigg[& \left(\frac{k_y^2}{k_\parallel^2}\frac{v_z k_z}{\eta(\boldsymbol{k})} + \frac{k_x^2}{k_\parallel^2}\sin q_{\boldsymbol{k}}\right)\tilde{\sigma}_z \\ & - \left(\frac{k_x^2}{k_\parallel^2}\frac{m(\boldsymbol{k})}{\eta(\boldsymbol{k})} + \frac{k_y^2}{k_\parallel^2}\cos q_{\boldsymbol{k}}\right)\tilde{\sigma}_y\Bigg], \end{aligned}\tag{A36}$$

$$\begin{aligned}\tilde{d}_y(\boldsymbol{k}) = \Delta\frac{k_x k_y}{k_\parallel^2}\Bigg[& \left(\sin q_{\boldsymbol{k}} - \frac{v_z k_z}{\eta(\boldsymbol{k})}\right)\tilde{\sigma}_z \\ & + \left(\cos q_{\boldsymbol{k}} - \frac{m(\boldsymbol{k})}{\eta(\boldsymbol{k})}\right)\tilde{\sigma}_y\Bigg], \end{aligned}\tag{A37}$$

$$\tilde{d}_z(\boldsymbol{k}) = -\Delta\frac{vk_x}{\eta(\boldsymbol{k})}\cos q_{\boldsymbol{k}}. \tag{A38}$$

Therefore, because of spin-orbit interaction, a spin singlet pair $\tilde{d}_0(\boldsymbol{k})$ is induced in the band basis, and the d-vector is rotated so that $\tilde{d}_y(\boldsymbol{k})$ and $\tilde{d}_z(\boldsymbol{k})$ become nonzero.

[1] M. Z. Hasan and C. L. Kane, Rev. Mod. Phys. **82**, 3045 (2010).
[2] X.-L. Qi and S.-C. Zhang, Rev. Mod. Phys. **83**, 1057 (2011).
[3] Y. Tanaka, N. Nagaosa, and M. Sato, J. Phys. Soc. Jpn. **81** (2012).
[4] A. P. Schnyder, S. Ryu, A. Furusaki, and A. W. W. Ludwig, Phys. Rev. B **78**, 195125 (2008).
[5] M. Sato, Phys. Rev. B **79**, 214526 (2009).
[6] M. Sato, Phys. Rev. B **81**, 220504(R) (2010).
[7] F. Wilczek, Nature Phys. **5**, 614 (2009).
[8] Y. Maeno, S. Kittaka, T. Nomura, S. Yonezawa, and

K. Ishida, J. Phys. Soc. Jpn **81**, 011009 (2012).
[9] A. Furusaki, M. Matsumoto, and M. Sigrist, Phys. Rev. B **64**, 054514 (2001).
[10] M. Stone and R. Roy, Phys. Rev. B **69**, 184511 (2004).
[11] S. Kashiwaya, H. Kashiwaya, H. Kambara, T. Furuta, H. Yaguchi, Y. Tanaka, and Y. Maeno, Phys. Rev. Lett. **107**, 077003 (2011).
[12] Y. Tanaka, T. Yokoyama, A. V. Balatsky, and N. Nagaosa, Phys. Rev. B **79**, 060505 (2009).
[13] M. Sato and S. Fujimoto, Phys. Rev. B **79**, 094504 (2009).
[14] M. Sato, Y. Takahashi, and S. Fujimoto, Phys. Rev. Lett. **103**, 020401 (2009).
[15] M. Sato, Y. Takahashi, and S. Fujimoto, Phys. Rev. B **82**, 134521 (2010).
[16] M. Sato and S. Fujimoto, Phys. Rev. Lett. **105**, 217001 (2010).
[17] J. D. Sau, R. M. Lutchyn, S. Tewari, and S. Das Sarma, Phys. Rev. Lett. **104**, 040502 (2010).
[18] J. Alicea, Phys. Rev. B **81**, 125318 (2010).
[19] R. M. Lutchyn, J. D. Sau, and S. Das Sarma, Phys. Rev. Lett. **105**, 077001 (2010).
[20] Y. Oreg, G. Refael, and F. von Oppen, Phys. Rev. Lett. **105**, 177002 (2010).
[21] R. M. Lutchyn, T. D. Stanescu, and S. Das Sarma, Phys. Rev. Lett. **106**, 127001 (2011).
[22] J. Alicea, Y. Oreg, G. Rafael, F. von Oppen, and M. F. Fisher, Nature Phys. **7**, 412 (2011).
[23] L. Fu and C. L. Kane, Phys. Rev. Lett. **100**, 096407 (2008).
[24] L. Fu and C. L. Kane, Phys. Rev. Lett. **102**, 216403 (2009).
[25] A. R. Akhmerov, J. Nilsson, and C. W. J. Beenakker, Phys. Rev. Lett. **102**, 216404 (2009).
[26] K. T. Law, P. A. Lee, and T. K. Ng, Phys. Rev. Lett. **103**, 237001 (2009).
[27] Y. Tanaka, T. Yokoyama, and N. Nagaosa, Phys. Rev. Lett. **103**, 107002 (2009).
[28] J. Linder, Y. Tanaka, T. Yokoyama, A. Sudbø, and N. Nagaosa, Phys. Rev. Lett. **104**, 067001 (2010).
[29] A. Yamakage, K. Yada, M. Sato, and Y. Tanaka, Phys. Rev. B **85**, 180509 (2012).
[30] A. Yamakage, Y. Tanaka, and N. Nagaosa, Phys. Rev. Lett. **108**, 087003 (2012).
[31] C. W. J. Beenakker, arXiv (2011), 1112.1950.
[32] Y. S. Hor, A. J. Williams, J. G. Checkelsky, P. Roushan, J. Seo, Q. Xu, H. W. Zandbergen, A. Yazdani, N. P. Ong, and R. J. Cava, Phys. Rev. Lett. **104**, 057001 (2010).
[33] S. Sasaki, M. Kriener, K. Segawa, K. Yada, Y. Tanaka, M. Sato, and Y. Ando, Phys. Rev. Lett. **107**, 217001 (2011).
[34] C. R. Hu, Phys. Rev. Lett. **72**, 1526 (1994).
[35] Y. Tanaka and S. Kashiwaya, Phys. Rev. Lett. **74**, 3451 (1995).
[36] S. Kashiwaya and Y. Tanaka, Rep. Prog. Phys. **63**, 1641 (2000).
[37] L. Hao and T. K. Lee, Phys. Rev. B **83**, 134516 (2011).
[38] T. H. Hsieh and L. Fu, Phys. Rev. Lett. **108**, 107005 (2012).
[39] G. Koren, T. Kirzhner, E. Lahoud, K. B. Chashka, and A. Kanigel, Phys. Rev. B **84**, 224521 (2011), 1111.3445.
[40] G. Koren and T. Kirzhner, arXiv (2012), 1207.5352.
[41] L. A. Wray, S.-Y. Xu, Y. Xia, D. Qian, A. V. Fedorov, H. Lin, A. Bansil, L. Fu, Y. S. Hor, R. J. Cava, et al., Nature Phys. **6**, 855 (2010).
[42] L. A. Wray, S. Xu, Y. Xia, D. Qian, A. V. Fedorov, H. Lin, A. Bansil, L. Fu, Y. S. Hor, R. J. Cava, et al., Phys. Rev. B **83**, 224516 (2011).
[43] M. Kriener, K. Segawa, Z. Ren, S. Sasaki, and Y. Ando, Phys. Rev. Lett. **106**, 127004 (2011).
[44] M. Kriener, K. Segawa, Z. Ren, S. Sasaki, S. Wada, S. Kuwabata, and Y. Ando, Phys. Rev. B **84**, 054513 (2011).
[45] P. Das, Y. Suzuki, M. Tachiki, and K. Kadowaki, Phys. Rev. B **83**, 220513 (2011).
[46] M. Kriener, K. Segawa, S. Sasaki, and Y. Ando, arXiv (2012), 1206.6260.
[47] Y. Nagai, H. Nakamura, and M. Machida, arXiv (2012), 1206.0563.
[48] L. Fu and E. Berg, Phys. Rev. Lett. **105**, 097001 (2010).
[49] H. Zhang, C.-X. Liu, X.-L. Qi, X. Dai, Z. Fang, and S.-C. Zhang, Nature Phys. **5**, 438 (2009).
[50] C.-X. Liu, X.-L. Qi, H. Zhang, X. Dai, Z. Fang, and S.-C. Zhang, Phys. Rev. B **82**, 045122 (2010).
[51] H. Padamsee, J. E. Neighbor, and C. A. Shiffman, J. Low Temp, Phys. **12**, 387 (1973).
[52] B. Mühlschlegel, Z. Phys. **155**, 313 (1959).
[53] D. Maruyama, M. Sigrist, and Y. Yanase, J. Phys. Soc. Jpn. **81**, 034702 (2012).